Three-dimensional thermal convection of viscoelastic fluids

Zhenyu Li and Roger E. Khayat*
Department of Mechanical and Materials Engineering, The University of Western Ontario, London, Ontario, Canada N6A 5B9
(Received 18 February 2005; published 17 June 2005)

The influence of inertia and elasticity on the onset and stability of three-dimensional thermal convection is examined for highly elastic polymeric solutions with constant viscosity. These solutions are known as Boger fluids, and their rheology is approximated by the Oldroyd-B constitutive equation. The onset and the stability of steady convective patterns, namely rolls, hexagons and squares, are studied in the post-critical range of the Rayleigh number by using an amplitude equation approach. The square pattern is found to be unstable. In contrast to Newtonian fluids, the hexagonal pattern can be stable for a certain range of elasticity.

DOI: 10.1103/PhysRevE.71.066305 PACS number(s): 47.20.Bp

I. INTRODUCTION

Thermal convection is a common and important phenomenon in nature, e.g., the dynamic motion of the oceans, the atmosphere, and the interior of stars and planets. It is also important in numerous industrial processes. It usually occurs in spatially extended systems when a sufficiently steep temperature gradient is applied across a fluid layer. Intensive experiments on instability caused by heating a very thin layer (a millimeter or less) of fluid with a free surface were conducted by Bénard [1]. Hexagonal cells were observed when the convection developed. Stimulated by these experiments, Rayleigh [2] derived the theoretical requirements for the development of convective motion in a layer of fluid with two free surfaces. He showed that the instability would occur when the adverse vertical temperature gradient was large enough. Later experiments on thermal convection in thicker layers (with or without a free surface) revealed the presence of convective cells of many forms not just hexagonal. The simplest convection pattern observed in laboratory is that of straight, parallel rolls when a horizontal thin fluid layer is confined between two thermally well conducting, parallel plates. Such rolls can be found near onset of convection. However, as the temperature gradient increases, the patterns often become progressively more complicated and more interesting [3].

While the problem of Rayleigh-Bénard (RB) thermal convection has been extensively investigated for Newtonian fluids, relatively little attention has been devoted to the thermal convection of viscoelastic fluids. Flow instability and turbulence are far less widespread in viscoelastic fluids than in Newtonian fluids because of the high viscosity of polymeric fluids. Green [4], Vest and Arpaci [5], and Sokolov and Tanner [6] conducted the linear stability analysis of RB convection of an upper-convected Maxwell fluid. Nonlinear RB convection of non-Newtonian fluids was considered by Eltayeb [7], Rosenblatt [8], Martinez-Mardones and Pérez-Garçia [9], Harder [10], and more recently by Khayat [11–14], Park and Lee [15], Martinez-Mardones *et al.* [16], and Parmentier, Lebon, and Regnier [17].

Some of the earlier experiments on the thermal convection of non-Newtonian fluids were conducted by Liang and Acrivos [18]. Their study, however, focused on the effects of shear thinning, which were found to enhance regularity in flow pattern. Kolodner [19] reported on and referred to recent experiments on the elastic behavior of individual, long strands of DNA in buffer solutions, which seem to indicate the convective patterns take the form of spatially localized standing and traveling waves that exhibit small amplitude and extremely long oscillation periods. The critical Rayleigh number for the onset of overstability is lower than for a Newtonian fluid, which is in agreement with linear stability analysis of viscoelastic fluids. Although both experiment [19] and theory [17] indicate that two-dimensional rolls are favored at the onset of oscillatory or stationary convection, the emergence of three-dimensional patterns can be important. The prevalence of two-dimensional rolls, similarly to Newtonian flow, should be expected only near the onset, where the velocity gradients and therefore normal stresses are weak.

The linear stability analysis predicts the threshold for the onset of stationary or oscillatory RB convection. Once the instability threshold is obtained, the amplitude of the motion, the preferred pattern, the size of convective cells, and whether the nonlinear RB convection are unique or not can only be found via nonlinear analysis. The objective of the present study is to investigate the onset and stability of flow patterns in viscoelastic RB convection. A weakly nonlinear approach, amplitude equation method, is adopted. The solutions of temperature, velocity, and stress components are expressed as series expansions in terms of the eigenfunctions of the linearized problem. These expansions are then substituted into the nonlinear equations and projected onto the eigenfunctions of the linear adjoint problem. This procedure results in an infinite set of ordinary differential equations that are then truncated by considering only a few sets of eigenfunctions.

II. PROBLEM FORMULATION

Consider an incompressible fluid confined between two infinite and flat plates at $Z=-D/2$ and $Z=D/2$. Let T_0 and $T_0+\delta T$ be the temperatures of the upper and lower plates,

*Corresponding author. Electronic address: rkhayat@uwo.ca

respectively, with T_0 being the reference temperature and δT being the temperature difference. In the present study, the fluid is assumed to obey the following equation of state:

$$\rho(T) = \rho_0[1 - \alpha_T(T - T_0)], \tag{1}$$

where ρ and ρ_0 are the densities at the temperatures T and T_0, respectively, and α_T is the coefficient of volumetric expansion. Let D, D^2/κ, κ/D, $\rho_0\kappa^2/D^2$, be, respectively, typical length, time, velocity and pressure, and $\eta\kappa/D^2$ be the typical stress. Here κ is the thermal diffusivity and η is the fluid viscosity. If the Boussinesq's approximation [20] is assumed to hold, then the dimensionless equations for the conservation of mass, momentum, and energy, read, respectively

$$\nabla \cdot \mathbf{u} = 0, \tag{2}$$

$$\mathrm{Pr}^{-1}(\mathbf{u}_{,t} + \mathbf{u} \cdot \nabla \mathbf{u}) = -\nabla p + \theta \mathbf{e}_z + \frac{Rv}{Rv+1}\Delta \mathbf{u} + \nabla \cdot \boldsymbol{\tau}, \tag{3}$$

$$\theta_{,t} + \mathbf{u} \cdot \nabla \theta = \Delta\theta + \mathrm{Ra}\, \mathbf{u} \cdot \mathbf{e}_z, \tag{4}$$

where ∇ is the gradient operator, and $\Delta = \nabla \cdot \nabla$ is the Laplacian operator. A subscript after a comma denotes partial differentiation. t is the time, $\mathbf{u} = (u, v, w)$ is the velocity vector, p is the pressure deviation from the steady state, and $\mathbf{e}_z$ is the unit vector in direction opposite to gravity. $\theta = g\alpha_T D^3(T - T_s)/\nu\kappa$ is the departure from the steady-state temperature, $T_s = T_0 - (Z/D - 1/2)\delta T$, where g is the acceleration due to gravity, and $\nu = \eta/\rho_0$ is the kinematic viscosity. In this work, the fluids examined are highly elastic polymeric solutions with constant viscosity η and a single relaxation time λ. These solutions are known as Boger fluids, and their rheology is approximated by the Oldroyd-B constitutive equation [21]. The elastic part of the deviatoric stress tensor $\boldsymbol{\tau}$ is given by

$$E[\boldsymbol{\tau}_{,t} + \mathbf{u} \cdot \nabla \boldsymbol{\tau} - (\nabla \mathbf{u})^T \cdot \boldsymbol{\tau} - \boldsymbol{\tau} \cdot \nabla \mathbf{u}] = -\boldsymbol{\tau} + \frac{1}{Rv+1}[\nabla \mathbf{u} + (\nabla \mathbf{u})^T], \tag{5}$$

where a superscript T denotes matrix transposition. There are four important dimensionless parameters in the problem, namely the Rayleigh number Ra, the Prandtl number Pr, the elasticity number E, and the solvent-to-solute viscosity ratio Rv:

$$\mathrm{Ra} = \frac{\delta T g \alpha_T D^3}{\nu\kappa}, \quad \mathrm{Pr} = \frac{\nu}{\kappa}, \quad E = \frac{\lambda\kappa}{D^2}, \quad Rv = \frac{\eta_s}{\eta_p}. \tag{6}$$

In this study, the stress free boundary conditions at the plates are considered, which is given by

$$w = \theta = \frac{\partial^2 w}{\partial z^2} = 0, \quad \text{at } z = -1/2, 1/2. \tag{7}$$

With the exception of density, the fluid parameters are assumed to be independent of temperature. In contrast to Taylor-Couette flow [22], the influence of temperature on rheological parameters, namely the relaxation time and viscosity, is not expected to be significant. The major influence of temperature for Taylor-Couette flow is of dissipative nature, which is bound to be significant given the relatively high critical Taylor or Deborah number at the onset of instability. Thermal convection of polymeric fluids can happen at relatively low temperature gradient or Rayleigh number. Chewing-gum solutions can boil at room temperature. More importantly, while the base state for Taylor-Couette flow is a purely azimuthal flow, that for Rayleigh-Bénard convection is pure heat conduction. Thus the absence of flow in the base state makes the influence of dissipation, and therefore the temperature dependence of the rheological parameters, essentially negligible.

III. LINEARIZED EIGENVALUE PROBLEM

The instability threshold of the conductive state can be found by performing a linear stability analysis. This is done by imposing infinitesimal perturbations $\mathbf{f}'(x,y,z,t)$ on the basic time-independent solution $\mathbf{f}_0(x,y,z)$,

$$\mathbf{f}(x,y,z,t) = \mathbf{f}_0(x,y,z) + \mathbf{f}'(x,y,z,t), \tag{8}$$

where supervector $\mathbf{f} = (\mathbf{u}, p, \theta, \boldsymbol{\tau})^T$. For RB convection, the basic solution $\mathbf{f}_0(x,y,z)$ is simply zero because the fluid remains in pure conduction state. After substituting expression (8) into the governing equations (2)–(5), the linearized governing equations are obtained by dropping any nonlinear terms of the infinitesimal perturbations. The solutions of the linearized equations are expressed in the form of normal modes as the following:

$$\mathbf{f}'(x,y,z,t) = \mathbf{F}(z) e^{i\mathbf{k}\cdot(x\mathbf{e}_x + y\mathbf{e}_y) + st}, \tag{9}$$

where $\mathbf{F}(z) = \{\mathbf{U}(z), P(z), \Theta(z), \mathbf{T}(z)\}^T$, $\mathbf{k}$ is the disturbance wave-number vector, and $s = s_R + i s_I$ is the complex eigenvalue dictating the time evolution of the disturbances. After substitution of expression (9) into the linearized equations, the resulting eigenvalue problem are written in a compact form as the following:

$$sM[\mathbf{F}(z) e^{i\mathbf{k}\cdot(x\mathbf{e}_x + y\mathbf{e}_y)}] = L[\mathbf{F}(z) e^{i\mathbf{k}\cdot(x\mathbf{e}_x + y\mathbf{e}_y)}]. \tag{10}$$

The explicit expressions of linear operators L and M are given, respectively, by

$$L = \begin{vmatrix} \frac{Rv}{Rv+1}\Delta & -\nabla & \mathbf{e}_z & \nabla \cdot \\ \nabla \cdot & 0 & 0 & 0 \\ \mathrm{Ra}\mathbf{e}_z \cdot & 0 & \Delta & 0 \\ \frac{1}{Rv+1}\Gamma & 0 & 0 & -1 \end{vmatrix}, \tag{11}$$

$$M = \begin{vmatrix} \mathrm{Pr}^{-1}\mathbf{I}_3 & 0 & 0 & 0 \\ 0 & 0 & 0 & 0 \\ 0 & 0 & 1 & 0 \\ 0 & 0 & 0 & E \end{vmatrix}, \tag{12}$$

where Γ stands for the operator $\Gamma = \nabla(\cdot) + \nabla^T(\cdot)$. Upon eliminating the pressure and the stress components, it is directly

checked that only two quantities, namely $\Theta(z)$ and $W(z)$, are relevant and the following set of coupled ordinary differential equations are obtained:

$$\left(\frac{d^2}{dz^2} - k^2 - s\right)\Theta(z) + W(z) = 0, \tag{13}$$

$$\left(\frac{d^2}{dz^2} - k^2 - \mathrm{Pr}^{-1}s\frac{(sE+1)(Rv+1)}{sERv+Rv+1}\right)\left(\frac{d^2}{dz^2} - k^2\right)W(z) = \frac{(sE+1)(Rv+1)}{sERv+Rv+1}\mathrm{Ra}k^2\Theta(z), \tag{14}$$

where $k=\sqrt{(k_x)^2+(k_y)^2}$ represents the magnitude of the wave-number vector **k**. This system reduces to Eqs. (8.37)–(8.39) in Drazin and Reid's monograph [23] in the case of Newtonian fluids, that is in the limit of $Rv \to \infty$. Note the difference in the scaling of the temperature. The corresponding free-free boundary conditions are given by

$$\Theta(z) = W(z) = \frac{d^2W(z)}{dz^2} = 0 \quad \text{at } z = -1/2, 1/2. \tag{15}$$

The solutions for the temperature and velocity coefficients are expressed in trigonometric functions

$$\Theta(z) = \sum_{n=1}^{\infty}\Theta_n \sin(n\pi z), \quad W(z) = \sum_{n=1}^{\infty} W_n \sin(n\pi z), \tag{16}$$

where Θ_n and W_n are now constants. For nontrivial solutions, the following characteristic equation results, namely

$$s^3 + \left(\frac{Rv}{Rv+1}\mathrm{Pr} + \frac{1}{(k^2+n^2\pi^2)E} + 1\right)s^2 + \left(\frac{Rv}{Rv+1}\mathrm{Pr} + \frac{\mathrm{Pr}+1}{(k^2+n^2\pi^2)E} - \frac{\mathrm{Pr}\,k^2\mathrm{Ra}}{(k^2+n^2\pi^2)^3}\right)s + \frac{\mathrm{Pr}}{(k^2+n^2\pi^2)E}\left(1 - \frac{k^2\mathrm{Ra}}{(k^2+n^2\pi^2)^3}\right) = 0. \tag{17}$$

It is not difficult to establish, as in the case of a Newtonian fluid, that the value of the Rayleigh number for the onset of stationary convection ($s=0$) is equal to $(\pi^2+k^2)^3/k^2$ for the most dominant mode. The critical (smallest) Rayleigh number and the corresponding wave number are equal to $\mathrm{Ra}_C^S = 27\pi^4/4$ and $k_C^S = \pi/\sqrt{2}$, respectively. The value of the critical Rayleigh number is independent of fluid elasticity or viscosity ratio due to the absence of base flow in RB convection. This result is in agreement with the experiments of Liang and Acrivos [18] and the linear stability analysis of Rosenblatt [8]. The onset of oscillatory convection coincides with the emergence of a pair of imaginary eigenvalues in the characteristic equation (17). Thus it can be deduced that the Rayleigh number corresponding to the onset of oscillatory convection is given by

$$\mathrm{Ra}^h = \frac{(k^2+\pi^2)^3\left(Rv\ \mathrm{Pr} + \frac{Rv+1}{(k^2+\pi^2)E}\right)\left[Rv\ \mathrm{Pr} + \left(\frac{\mathrm{Pr}+1}{(k^2+\pi^2)E}+1\right)(Rv+1)\right]}{(Rv\ \mathrm{Pr}+Rv+1)(Rv+1)\mathrm{Pr}\,k^2}, \tag{18}$$

from which the critical (smallest) value can only be obtained numerically. Due to the mathematical complexity of the oscillatory convection in the post-critical range of the Rayleigh number, $\mathrm{Ra} > \mathrm{Ra}_C^S$, this study will focus on the stability of different stationary convective patterns.

IV. AMPLITUDE EQUATIONS

An amplitude equation approach is used to asses the stability of three convection patterns, namely rolls, hexagons, and squares, in the post-critical range, $\mathrm{Ra} > \mathrm{Ra}_C^S$. Readers are referred to Friedman [24], Eckhaus [25], Newell *et al.* [26], and Cross and Hohenberg [27] for the general theory. The current derivation follows closely that developed by Parmentier *et al.* [17], and is only reviewed. The current amplitude equations are, however, obtained more accurately as certain terms dropped by Parmentier *et al.* [17] are included here.

Equations (2)–(5) are rewritten compactly as

$$NL(\mathbf{f}) = L_C(\mathbf{f}) + L_\Delta(\mathbf{f}). \tag{19}$$

The explicit expressions of operators L_C and L_Δ are given, respectively, by

$$L_C = \begin{vmatrix} \frac{Rv}{Rv+1}\Delta & -\nabla & \mathbf{e}_z & \nabla\cdot \\ \nabla\cdot & 0 & 0 & 0 \\ \mathrm{Ra}_c^s\mathbf{e}_z\cdot & 0 & \Delta & 0 \\ \frac{1}{Rv+1}\Gamma & 0 & 0 & -1 \end{vmatrix},$$

$$L_\Delta = \begin{vmatrix} 0 & 0 & 0 & 0 \\ 0 & 0 & 0 & 0 \\ (\mathrm{Ra}-\mathrm{Ra}_c^s)\mathbf{e}_z\cdot & 0 & 0 & 0 \\ 0 & 0 & 0 & 0 \end{vmatrix}. \tag{20}$$

$NL(f)$ represents the nonlinear and the time-rate contributions, namely

$$NL(\mathbf{f}) = \begin{vmatrix} \mathrm{Pr}^{-1}(\mathbf{u}_{,t} + \mathbf{u}\cdot\boldsymbol{\nabla}\,\mathbf{u}) \\ 0 \\ \theta_{,t} + \mathbf{u}\cdot\boldsymbol{\nabla}\,\theta \\ E[\boldsymbol{\tau}_{,t} + \mathbf{u}\cdot\boldsymbol{\nabla}\,\boldsymbol{\tau} - (\boldsymbol{\nabla}\mathbf{u})^{\mathrm{T}}\cdot\boldsymbol{\tau} - \boldsymbol{\tau}\cdot\boldsymbol{\nabla}\,\mathbf{u}] \end{vmatrix}. \quad (21)$$

The method of solution consists of expanding $\mathbf{f}$ in terms of eigenfunctions of the linear problem in the form

$$\mathbf{f} = \sum_{p_1=1}^{\infty}\sum_{q_1} A_{q_1}^{p_1}(t)\mathbf{f}_{q_1}^{p_1}(x,y,z), \quad p_1 = 1,2,\ldots,\infty;$$
$$q_1 = \pm N,\ldots,\pm 2,\pm 1. \quad (22)$$

The summation over q_1 extends on the whole set of allowable wave vectors $\mathbf{k}_{q_1}$, which in the case of an infinite horizontal extent can take all possible directions and moduli, while the summation over p_1 runs over the whole set of eigenfunctions pertaining to a given wave vector $\mathbf{k}_{q_1}$. $A_{q_1}^{p_1}(t)$ designates the amplitude of the mode and must satisfy $A_{q_1}^{p_1} = A_{-q_1}^{\bar{p}_1}$ in order that $\mathbf{f}$ be real, a bar over a symbol means complex conjugate. The eigenfunctions $\mathbf{f}_{q_1}^{p_1}(x,y,z)$ are solutions of the linearized problems defined by

$$s_{q_1}^{p_1} M(\mathbf{f}_{q_1}^{p_1}(x,y,z)) = L_{\mathrm{C}}(\mathbf{f}_{q_1}^{p_1}(x,y,z)), \quad (23)$$

where L_{C} is given by Eq. (20) while operator M is expressed by Eq. (12).

The eigenvalues $s_{q_1}^{p_1}$ of the linearized problem are ordered in such a way that $\mathrm{Re}(s_{q_1}^1) > \mathrm{Re}(s_{q_1}^2) > \cdots > \mathrm{Re}(s_{q_1}^n)$, where $\mathrm{Re}(s)$ stands for the real part of s. Solutions $\mathbf{f}_{q_1}^{p_1}(x,y,z)$ are sought of the form

$$\mathbf{f}_{q_1}^{p_1}(x,y,z) = \mathbf{F}_{q_1}^{p_1}(z)\exp[i\mathbf{k}^{q_1}\cdot(\mathbf{e}_x x + \mathbf{e}_y y)], \quad (24)$$

where $\mathbf{e}_x$ and $\mathbf{e}_y$ are unit vectors in the x and y directions, respectively. $\mathbf{F}_{q_1}^{p_1}(z) = \{\mathbf{U}_{q_1}^{p_1}(z), P_{q_1}^{p_1}(z), \Theta_{q_1}^{p_1}(z), \mathbf{T}_{q_1}^{p_1}(z)\}^{\mathrm{T}}$, and is determined after substitution of expression (24) back into Eq. (23).

The next step of the procedure consists of projecting the nonlinear equation (19) on the eigenfunctions $\mathbf{f}_{q_2}^{*p_2}(x,y,z)$ of *the linear adjoint* problem, which is formulated in Appendix A. This leads to

$$\langle NL(\mathbf{f}), \mathbf{f}_{q_2}^{*p_2}(x,y,z)\rangle = \langle L_{\mathrm{C}}(\mathbf{f}), \mathbf{f}_{q_2}^{*p_2}(x,y,z)\rangle + \langle L_{\Delta}(\mathbf{f}), \mathbf{f}_{q_2}^{*p_2}(x,y,z)\rangle. \quad (25)$$

Here a bracket denotes the average integral of the scalar product defined by

$$\langle a,b\rangle \equiv \lim_{L\to\infty}\frac{1}{4L^2}\int_{\mathrm{v}} P_{\mathrm{v}}(a,b)\,dx\,dy\,dz, \quad (26)$$

where P_{v} is scalar product defined on the volume v. Equation (25) stands for an infinite number of ordinary differential equations for the unknown amplitudes $A_{q_1}^{p_1}(t)$. After integration by parts and using relation (23), the infinite sequence of amplitude equations are obtained as the following:

$$A_{q_1,t}^{p_1} C_0(q_1,p_1) = s_{q_1}^{p_1} C_0(q_1,p_1) A_{q_1}^{p_1} + (r-1)\sum_{p_2}^{\infty} C_1(q_1,p_1,p_2) A_{q_1}^{p_2}$$
$$- \sum_{p_2,p_3}^{\infty}\sum_{q_2,q_3} \delta(\mathbf{k}^{-q_1}\mathbf{k}^{q_2}\mathbf{k}^{q_3}) C_2\begin{pmatrix} p_1,p_2,p_3 \\ q_1,q_2,q_3 \end{pmatrix}$$
$$\times A_{q_2}^{p_2} A_{q_3}^{p_3}, \quad (27)$$

where $r = \mathrm{Ra}/\mathrm{Ra}_{\mathrm{C}}^{\mathrm{S}}$ is the reduced Rayleigh number, which will be used as the control parameter instead of Ra. The δ function is defined by

$$\delta(\mathbf{k}^{-p_1}\mathbf{k}^{p_2}\mathbf{k}^{p_3}) = \begin{cases} 0 & \mathbf{k}^{-p_1} + \mathbf{k}^{p_2} + \mathbf{k}^{p_3} \neq 0 \\ 1 & \mathbf{k}^{-p_1} + \mathbf{k}^{p_2} + \mathbf{k}^{p_3} = 0 \end{cases}.$$

The coefficients C_0, C_1, and C_2 are given by

$$C_0(q_1,p_1) = \mathrm{Pr}^{-1}\langle \mathbf{U}_{q_1}^{p_1}(z), \mathbf{U}_{q_1}^{*p_1}(z)\rangle + \langle \Theta_{q_1}^{p_1}(z), \Theta_{q_1}^{*p_1}(z)\rangle$$
$$+ E\langle \mathbf{T}_{q_1}^{p_1}(z), \mathbf{T}_{q_1}^{*p_1}(z)\rangle, \quad (28)$$

$$C_1(q_1,p_1,p_2) = \mathrm{Ra}_{\mathrm{C}}^{\mathrm{S}}\langle \Theta_{q_1}^{p_2}(z), W_{q_1}^{*p_1}(z)\rangle, \quad (29)$$

$$C_2\begin{pmatrix} p_1,p_2,p_3 \\ q_1,q_2,q_3 \end{pmatrix} = \mathrm{Pr}^{-1}\langle \mathbf{U}_{q_3}^{p_3}(z)\cdot\boldsymbol{\nabla}\,\mathbf{U}_{q_2}^{p_2}(z), \mathbf{U}_{q_1}^{*p_1}(z)\rangle$$
$$+ \langle \mathbf{U}_{q_3}^{p_3}(z)\cdot\boldsymbol{\nabla}\,\Theta_{q_2}^{p_2}(z), \Theta_{q_1}^{*p_1}(z)\rangle$$
$$+ E\langle \mathbf{U}_{q_3}^{p_3}(z)\cdot\boldsymbol{\nabla}\,\mathbf{T}_{q_2}^{p_2}(z), \mathbf{T}_{q_1}^{*p_1}(z)\rangle$$
$$- E\langle \boldsymbol{\nabla}^{\mathrm{T}}\mathbf{U}_{q_3}^{p_3}(z)\cdot\mathbf{T}_{q_2}^{p_2}(z), \mathbf{T}_{q_1}^{*p_1}(z)\rangle$$
$$- E\langle \mathbf{T}_{q_3}^{p_3}(z)\cdot\boldsymbol{\nabla}\,\mathbf{U}_{q_2}^{p_2}(z), \mathbf{T}_{q_1}^{*p_1}(z)\rangle. \quad (30)$$

It is, of course, highly desirable to reduce the infinite number of nonlinear coupled ordinary differential equations to a finite set of equations. This will be achieved by separating the set of eigenmodes $\mathbf{f}_{q_1}^{p_1}(x,y,z)$ in two subsets K_{C} and K_{S}. The subset K_{C} contains the critical eigenmodes with a zero growth rate $[\mathrm{Re}(s_{q_1}^{p_1}) = 0]$. The critical eigenmodes are the ones corresponding to $p_1 = 1$ and $|k_{q_1}| = k_{\mathrm{C}}^{\mathrm{S}}$, with $k_{\mathrm{C}}^{\mathrm{S}}$ being the critical wave number at the onset of stationary convection. Since the stability of hexagonal, square, and roll cells is studied, it is sufficient to consider 12 wave-number vectors $k_{q_1}(q_1 = \pm 1, \pm 2, \ldots, \pm 6)$ distributed on a circumference of radius $k_{\mathrm{C}}^{\mathrm{S}}$ and making an angle of 30° between each other (see Fig. 6 in Parmentier *et al.* [17]). It follows that the 12 critical eigenmodes are $\mathbf{f}_{q_1}^1(x,y,z)$, $q_1 = \pm 1, \pm 2, \ldots, \pm 6$. The subset K_{S} consists of all stable eigenmodes characterized by a negative growth rate $[\mathrm{Re}(s_{q_1}^{p_1}) < 0]$. In a weakly nonlinear regime, these stable eigenmodes are rapidly relaxing from which it follows that the amplitudes in Eq. (27) corresponding to these stable modes can be notably simplified. It is justified to drop in Eq. (27) the term containing the time derivative because these modes are quickly damped. Thus the following relation between the stable and the critical modes is obtained:

$$A_{q_1}^{p_1} = -(r-1)C_1(q_2,1,1)A_{q_2}^1 + \frac{1}{s_{q_1}^{p_1}C_0(q_1,p_1)}\sum_{q_2,q_3}\delta(\mathbf{k}^{-q_1}\mathbf{k}^{q_2}\mathbf{k}^{q_3})C_2\begin{pmatrix} p_1,1,1 \\ q_1,q_2,q_3 \end{pmatrix}A_{q_2}^1 A_{q_3}^1, \tag{31}$$

where q_2, $q_3 = \pm 1, \pm 2, \ldots, \pm 6$. Note that the first term on the right-hand side is not accounted for in the formulation of Parmentier *et al.* [17]. It follows from the above consideration that the infinite number of ordinary differential equations (27) reduce to a finite number of equations, namely

$$A_{q_1}^{p_1},_t C_0(q_1,1) = (r-1)\sum_{p_2}^{\infty} C_1(q_1,1,p_2)A_{q_1}^{p_2} - \sum_{p_2,p_3}^{\infty}\sum_{q_2,q_3}\delta(\mathbf{k}^{-q_1}\mathbf{k}^{q_2}\mathbf{k}^{q_3})C_2\begin{pmatrix} 1,p_2,p_3 \\ q_1,q_2,q_3 \end{pmatrix}A_{q_2}^{p_2}A_{q_3}^{p_3}, \tag{32}$$

where $q_1 = \pm 1, \pm 2, \ldots, \pm 6$. The number of modes p_2, p_3 is increased until a relative accuracy is reached. After substitution of Eq. (31) into Eq. (32) and omitting terms of order higher than 3 (this is justified as one remains in the weakly nonlinear regime), the following amplitude equations are obtained:

$$\tau_0\frac{dA_1}{dt} = (r-1)A_1 - b(|A_2|^2 + |A_3|^2)A_1 - c|A_1|^2A_1 - d(|A_6|^2 + |A_5|^2)A_1 - e|A_4|^2A_1, \tag{33}$$

$$\tau_0\frac{dA_2}{dt} = (r-1)A_2 - b(|A_1|^2 + |A_3|^2)A_2 - c|A_2|^2A_2 - d(|A_4|^2 + |A_6|^2)A_2 - e|A_5|^2A_2, \tag{34}$$

$$\tau_0\frac{dA_3}{dt} = (r-1)A_3 - b(|A_1|^2 + |A_2|^2)A_3 - c|A_3|^2A_3 - d(|A_4|^2 + |A_5|^2)A_3 - e|A_6|^2A_3, \tag{35}$$

$$\tau_0\frac{dA_4}{dt} = (r-1)A_4 - b(|A_5|^2 + |A_6|^2)A_4 - c|A_4|^2A_4 - d(|A_2|^2 + |A_3|^2)A_4 - e|A_1|^2A_4, \tag{36}$$

$$\tau_0\frac{dA_5}{dt} = (r-1)A_5 - b(|A_4|^2 + |A_6|^2)A_5 - c|A_5|^2A_5 - d(|A_1|^2 + |A_3|^2)A_5 - e|A_2|^2A_5, \tag{37}$$

$$\tau_0\frac{dA_6}{dt} = (r-1)A_6 - b(|A_4|^2 + |A_5|^2)A_6 - c|A_6|^2A_6 - d(|A_1|^2 + |A_2|^2)A_6 - e|A_3|^2A_6. \tag{38}$$

Here, τ_0 is the relaxation time, b, c, d, and e are complex coefficients that depend generally on Pr, Rv, E, and r, and are given explicitly in Appendix B. Equations (33)–(38) are usually referred to as the Landau equations [23]. Note that the superscripts have been omitted since all of them are equal to 1.

V. ROLL, HEXAGON, AND SQUARE CONVECTIVE PATTERNS

For a small value of E or a large value of Rv, one expects the behavior of the flow to be similar to the Newtonian regime, at least around the purely conductive state. Similarly to the case of a Newtonian fluid, one of the steady-state solution branches corresponds to pure heat conduction. As Ra exceeds a critical value, the conduction state loses its stability to steady convection. In contrast to Newtonian fluids, which admit only rolls in the post-critical range, viscoelastic convection can be in the form of rolls or hexagons depending on the level of elasticity (see below).

Parmentier *et al.* [17] carried out a weakly nonlinear stability analysis of Bénard-Marangoni convection of viscoelastic fluids using an amplitude-equation method. Three cell patterns consisting of rolls, hexagons, and squares have been examined for stationary convection; oscillatory convection was not considered. The roll pattern was predicted to be stable for only small elasticity number ($E < 0.0035$) near criticality, and the three-dimensional hexagonal pattern was found to be stable for $E \in [0.0035, 0.07]$, for a fluid with $\mathrm{Pr} = 1000$ and $Rv \approx 0.01$. The square pattern was found to be always unstable (at least near criticality). It is observed that, according to the current linear stability analysis, the limit $E = 0.07$ corresponds to the critical elasticity number for the emergence of oscillatory thermal convection.

In this section, the amplitude equations are used to examine parameter ranges for three-dimensional stationary convection that have not been covered by Parmentier *et al.* [17]. The stability of the steady rolls, hexagons, and squares is determined through linear stability analysis of the steady-state solutions of Eqs. (33)–(38) pertaining to each pattern. The current calculations are based on the free-free boundary conditions only, and indicate that the viscosity ratio has a strong influence on the stable ranges of stationary roll and hexagonal patterns. The square pattern is found to be always unstable. The stability picture is best illustrated in the (r, E) plane. Alternatively, the stability picture could be examined in the (r, De) plane, where De is the Deborah number. However, additional calculations (not included here) show that the De varies linearly with E, and, therefore no new qualitatively different insight would be gained. Figure 1 shows typically the regions of existence of roll and hexagonal patterns for a fluid with $Rv = 3.75$ and $\mathrm{Pr} = 1000$. In the figure, H and R denote stable hexagonal and roll regions, respectively. In contrast to the prediction of Parmentier *et al.* [17], there is no region where both hexagon and roll patterns coexist, as a result of the use of different boundary conditions here. Despite this discrepancy, qualitative agreement is obtained regarding the stable ranges of hexagonal and roll patterns. For relatively small E, the conductive state C is lost to two-dimensional stationary convection (rolls) when r exceeds unity. When the level of elasticity exceeds a critical value E^{H}, but remains smaller than E^{h} (elasticity level corresponding to the onset of oscillatory convection), only the hexago-

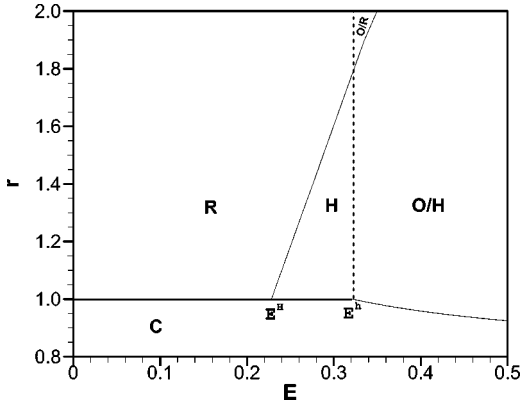

FIG. 1. Stability picture obtained with amplitude equation method for two convection patterns, namely roll and hexagon. This figure shows the stable range of roll and hexagonal patterns on (r,E) plane for a fluid with $\mathrm{Pr}=1000$ and $Rv=3.75$. H and R represent stable regions for hexagonal and roll patterns, respectively, C the stable heat conduction state, and O the oscillatory convection. E^{H} represents the critical elasticity number for the emergence of three-dimensional convective pattern (hexagon), while E^{h} is the elasticity level corresponding to the onset of oscillatory convection.

nal pattern is stable at the onset of stationary convection. Beyond E^{h}, oscillatory convection sets in. Thus inertia tends to enhance the onset of convective rolls. It is found that E^{H} increases linearly with r, which seems to be the case for other values of Rv and Pr. The figure also indicates that E^{H} can be larger than E^{h} at higher Rayleigh number, which means that both stationary roll and oscillatory convection become possible. This region is indicated by O/R in the figure. For $E>E^{\mathrm{h}}$, the conductive state loses its stability at $r<1$ as predicted by linear stability analysis. Similarly, there is a region marked by O/H, where both stationary hexagons and oscillatory convection are possible.

The dependence of E^{H} on the fluid parameters is summarized in Figs. 2 and 3, where E^{H} is plotted against Pr and Rv at $r=1.1$, respectively. Figure 2 shows the influence of Pr on E^{H} for $Rv\in[0,5]$. Two distinct regimes can be discerned from Fig. 2. For small Pr values, E^{H} drops sharply like $\mathrm{Pr}^{0.93}$ regardless of the viscosity ratio. In this range, the roll pattern

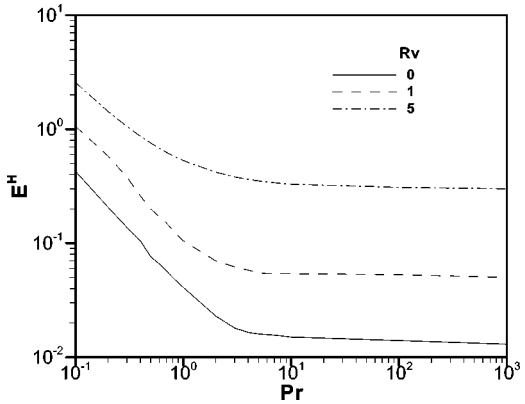

FIG. 2. Influence of Pr on the critical elasticity number E^{H} for different value of Rv. The curves show that E^{H} decreases monotonically with Pr.

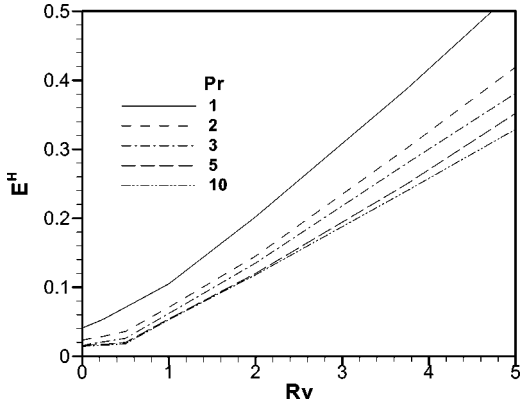

FIG. 3. Influence of Rv on the critical elasticity number E^{H} for different value of Pr. The curve show the linear dependence of E^{H} on Rv when $Rv>0.5$.

appears to be preferred unless E is relatively large. Thus rarefied gases ($\mathrm{Pr}\ll 1$ and $Rv=0$) would exhibit a predominantly roll pattern. For larger Pr values, E^{H} remains essentially constant. The curves become flattened, which indicates that for typical polymeric solutions ($\mathrm{Pr}\gg 1$), the influence of Pr on the stationary convective patterns is not significant. Thus it is the viscosity ratio of the polymeric solution that determines the likelihood for two- or three-dimensional convection. Note that E^{H} tends to infinity, for any Pr, in the limit of a Newtonian fluid ($Rv\to\infty$). This can be seen more clearly from Fig. 3, which shows the increase of E^{H} with Rv for several values of Pr. The increase is slow when Rv is relatively small. For large Rv, the figure indicates that E^{H} is simply proportion to Rv, and this behavior may be given by

$$E^{\mathrm{H}}\approx 0.07Rv-0.022 \quad (\mathrm{Pr}\gg 1). \tag{39}$$

Thus, similarly to elasticity, viscosity tends to precipitate the emergence of three-dimensional convection, as well as the onset of oscillatory behavior. There is thus a synergetic interplay between elastic and viscous effects regarding the loss of stability of the roll pattern. The stable range of two-dimensional roll pattern is significantly widened with increasing Rv, which is of course expected as the contribution of the Newtonian solvent increases. Recall, that in the Newtonian limit, only rolls are predicted, regardless of the nature of boundary conditions used [28].

Unlike the critical Rayleigh number $\mathrm{Ra}_{\mathrm{C}}^{\mathrm{S}}$ at the onset of stationary thermal convection, the amplitude of convection is strongly influenced by fluid elasticity, viscosity ratio, and Prandtl number. It is convenient to monitor the response of the Nusselt number Nu as Ra is increased in the post-critical range. The Nusselt number is defined in terms of the heat flux Q at the lower plate, averaged over a cell width:

$$\mathrm{Nu}=1-\frac{1}{\mathrm{Ra}}\langle\theta_{,z}(x,y,z=-1/2,t)\rangle=1 - \frac{1}{\mathrm{Ra}}\sum_{p}\sum_{q}A_{q}^{p}\Theta_{q}^{p}p\pi\cos\left(\frac{p\pi}{2}\right)\langle e^{ik_{q}(x\cdot\mathbf{e}_{x}+y\cdot\mathbf{e}_{y})}\rangle, \tag{40}$$

where $\langle\rangle$ denotes double integration over $x\in[0,2\pi/k]$ and $y\in[0,2\pi/k]$.

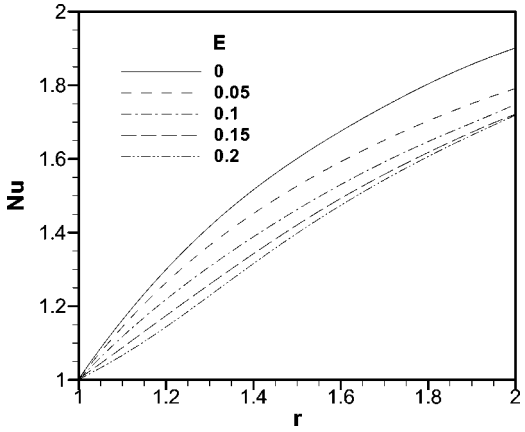

FIG. 4. Bifurcation diagrams and influence of elasticity on stationary thermal convection of roll patterns. The Nusselt number is plotted against the reduced Rayleigh number r for $E \in [0, 0.2]$ with $Rv = 3.75$ and Pr = 7.

The influence of fluid elasticity on the steady bifurcation picture of roll pattern is depicted in Fig. 4, where Nu is plotted against r for $E \in [0, 0.2]$, $Rv = 3.75$, and Pr = 7. E is chosen relatively small to insure that the exchange of stability between conductive state and stationary roll pattern is valid. The figure indicates that fluid elasticity tends to prohibit heat transport, relatively to a Newtonian fluid. The bifurcation is supercritical, reflecting a gradual increase in Nu as r exceeds slightly 1. Near the critical point, the influence of E is gradual, with Nu decreasing almost linearly as E increases. At higher r values, the drop in Nu between two successive E values is largest near $E = 0$. Thus elasticity appears to affect little the steady-state thermal convection for the higher Rayleigh number range. Physically, one expects the dependence of Nu on E to be continuous as the flow deviates from the Newtonian limit. At higher elasticity level, the conductive state loses its stability to stationary hexagonal convective pattern as r exceeds 1. The steady bifurcation picture of hexagonal pattern is also supercritical as depicted in Fig. 5, the plot of Nu against r for $E \in [0.2, 0.4]$, Rv

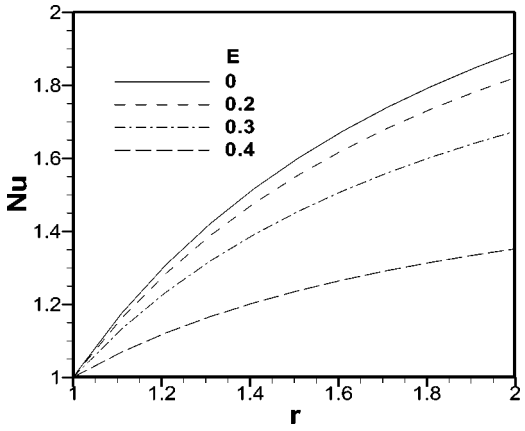

FIG. 5. Bifurcation diagrams and influence of viscosity ratio on stationary thermal convection of hexagonal patterns. The Nusselt number is plotted against the reduced Rayleigh number r for $E \in [0.2, 0.4]$ with $Rv = 3.75$ and Pr = 7.

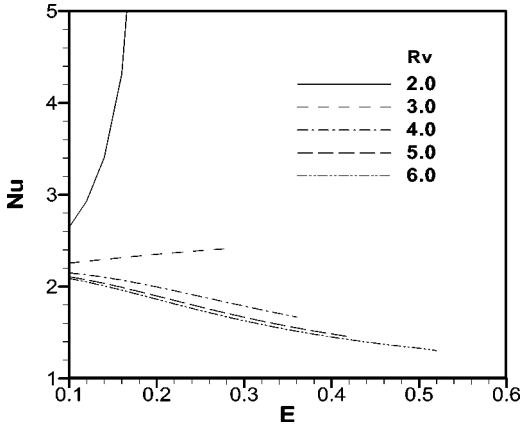

FIG. 6. Influence of elasticity on stationary thermal convection of hexagonal pattern. The Nusselt number is plotted against the elasticity number E for $r = 2$ with $Rv = 3.75$ and Pr = 7.

$= 3.75$, and Pr = 7. The drop in Nu between two successive E values becomes larger as r increasing, which indicates that elasticity affects much the steady-state thermal convection for the higher Rayleigh number range. For $Rv = 3.75$, elasticity tends to prohibit heat transport. However, this is not always the case. The heat transport is actually enhanced with increasing elasticity as depicted in Fig. 6, which is the plot of Nu against E for $Rv \in [2, 6]$, $r = 2$, and Pr = 10.

The influence of viscosity ratio on Nusselt number for steady roll pattern is shown in Fig. 7, which parallels the influence of elasticity as Rv decreases. Recall that as the (Newtonian) solvent viscosity decreases, the effective elasticity of the fluid becomes more significant. Indeed, the figure indicates that Nu decreases with decreasing Rv for a given r. Figures 4, 5, and 7 seem to suggest that there is little influence of fluid elasticity or relaxation on the amplitude of steady convection when r is close to 1. This observation is in agreement with the measurements of Liang and Acrivos [18]. It is important to observe that the physical significance of the branch curves in Figs. 4, 5, and 7 become clear only when the stability of these branches is known. It is found that Prandtl number has less influence on the amplitude of both

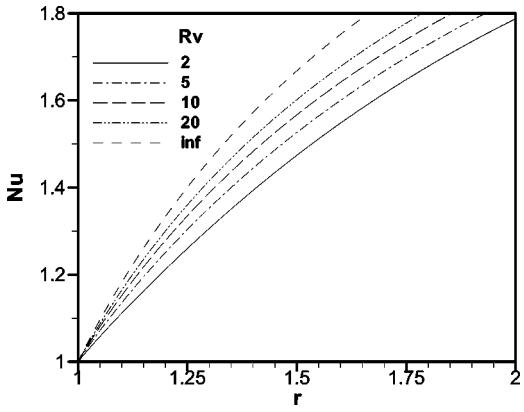

FIG. 7. Bifurcation diagrams and influence of viscosity ratio on stationary thermal convection of roll patterns. The Nusselt number is plotted against the reduced Rayleigh number r for $Rv \in [5, \infty]$ with $E = 0.1$ and Pr = 7.

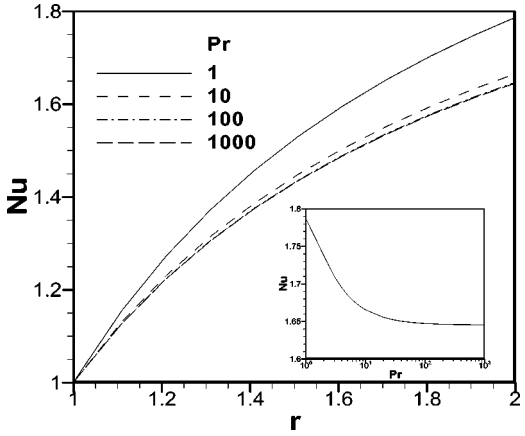

FIG. 8. Bifurcation diagrams and influence of Pr on stationary thermal convection of hexagonal patterns. The Nusselt number is plotted against the reduced Rayleigh number r for $\mathrm{Pr}\in[1,1000]$ with $Rv=3.75$ and $E=0.3$. The inset shows the asymptotic behavior of Nu against Pr.

roll and hexagonal convective patterns. For fixed elasticity number and viscosity ratio, the Nusselt number keeps essentially the same as Pr varies from 1 to 1000, as shown in Fig. 8, which is the plot of Nu for the steady hexagonal pattern against r for $E=0.3$ and $Rv=3.75$. The inset clearly shows an asymptotic behavior.

VI. CONCLUSION

The finite-amplitude thermal convection for a thin layer of a viscoelastic fluid of the Oldroyd-B type is examined in this study. An amplitude equation approach is used to study the stability of stationary convective patterns, namely rolls, hexagons, and squares, in the post-critical range of the Rayleigh number. Six Landau type amplitude equations are derived by following a generalized method proposed by Parmentier *et al.* [17]. Square patterns are found to be unstable for any parameter range. Steady hexagonal patterns are predicted to be stable for certain range of elasticity number, which is in contrast to the Newtonian case, where only rolls are predicted to be stable. The influence of the Prandtl number and the viscosity ratio on the stability of rolls and hexagons are examined. It is found that the viscosity ratio plays a more important role in determining the likelihood of the two- or three-dimensional patterns for typical polymeric solutions.

ACKNOWLEDGMENT

The financial support of the Natural Science and Engineering Research Council is gratefully acknowledged.

APPENDIX A: THE LINEAR ADJOINT PROBLEM

In this appendix, the derivation of the linear adjoint problem is briefly outlined. Readers are referred to Friedman [24] and Eckhaus [25] for the general theory. The linear adjoint problem is defined by

$$\langle L_{\mathrm{C}}(\mathbf{f})-sM(\mathbf{f}),\mathbf{f}^{*}\rangle=\langle\mathbf{f},L_{\mathrm{C}}^{*}(\mathbf{f}^{*})-s^{*}M^{*}(\mathbf{f}^{*})\rangle, \tag{A1}$$

where s^{*} and the supervector $\mathbf{f}^{*}=(\mathbf{u}^{*},p^{*},\theta^{*},\boldsymbol{\tau}^{*})^{\mathrm{T}}$ represent, respectively, the eigenvalue and eigenfunctions in the adjoint linear problem. L_{C}^{*} and M^{*} are the adjoint operators of L_{C} and M defined in Eqs. (18) and (23). Noting that

$$\begin{aligned}\langle sM(\mathbf{f}),\mathbf{f}^{*}\rangle&=\langle\mathrm{Pr}^{-1}s\mathbf{u},\mathbf{u}^{*}\rangle+\langle s\theta,\theta^{*}\rangle+\langle Es\boldsymbol{\tau},\boldsymbol{\tau}^{*}\rangle=\langle\mathbf{u},\mathrm{Pr}^{-1}s^{*}\mathbf{u}^{*}\rangle\\&+\langle\theta,s^{*}\theta^{*}\rangle+\langle\boldsymbol{\tau},Es^{*}\boldsymbol{\tau}^{*}\rangle=\langle\mathbf{f},s^{*}M^{*}(\mathbf{f}^{*})\rangle,\end{aligned} \tag{A2}$$

then it is readily found that M^{*} is given by

$$M^{*}=\begin{vmatrix}\mathrm{Pr}^{-1}&0&0&0\\0&0&0&0\\0&0&1&0\\0&0&0&E\end{vmatrix}. \tag{A3}$$

Similarly, noting that

$$\begin{aligned}\langle(\Delta\mathbf{u}),\mathbf{u}^{*}\rangle&=\langle\mathbf{u},(\Delta\mathbf{u}^{*})\rangle+\langle\boldsymbol{\nabla},(\mathbf{u}^{*}\cdot\boldsymbol{\nabla}\mathbf{u})\rangle-\langle\boldsymbol{\nabla},(\mathbf{u}\cdot\boldsymbol{\nabla}\mathbf{u}^{*})\rangle\\&=\langle\mathbf{u},(\Delta\mathbf{u}^{*})\rangle+\langle u_{z},u_{z}^{*}\rangle\big|_{0}^{1},\end{aligned} \tag{A4}$$

$$\langle-\boldsymbol{\nabla}p,\mathbf{u}^{*}\rangle=\langle p,\boldsymbol{\nabla}\cdot\mathbf{u}^{*}\rangle-\langle p,u_{z}^{*}\rangle\big|_{0}^{1}, \tag{A5}$$

$$\langle\theta\mathbf{e}_{z},\mathbf{u}^{*}\rangle=\langle\theta,\mathbf{u}^{*}\cdot\mathbf{e}_{z}\rangle, \tag{A6}$$

$$\langle\boldsymbol{\nabla}\cdot\boldsymbol{\tau},\mathbf{u}^{*}\rangle=-\langle\boldsymbol{\tau},\boldsymbol{\nabla}\mathbf{u}^{*}\rangle+\langle\mathbf{e}_{z}:\boldsymbol{\tau},\mathbf{u}^{*}\rangle\big|_{0}^{1}, \tag{A7}$$

$$\langle\boldsymbol{\nabla}\cdot\mathbf{u},p^{*}\rangle=-\langle\mathbf{u},\boldsymbol{\nabla}p^{*}\rangle, \tag{A8}$$

$$\langle\mathrm{Ra}\mathbf{u}\cdot\mathbf{e}_{z},\theta^{*}\rangle=\langle\mathbf{u},\mathrm{Ra}\theta^{*}\mathbf{e}_{z}\rangle, \tag{A9}$$

$$\langle\Delta\theta,\theta^{*}\rangle=\langle\theta,\Delta\theta^{*}\rangle+\left\langle\frac{\partial\theta}{\partial z},\theta^{*}\right\rangle\Bigg|_{0}^{1}, \tag{A10}$$

$$\langle-\boldsymbol{\tau},\boldsymbol{\tau}^{*}\rangle=-\langle\boldsymbol{\tau},\boldsymbol{\tau}^{*}\rangle, \tag{A11}$$

$$\langle a\dot{\boldsymbol{\gamma}},\boldsymbol{\tau}^{*}\rangle=\langle\mathbf{u},a[\boldsymbol{\nabla}\boldsymbol{\tau}^{*}+(\boldsymbol{\nabla}\boldsymbol{\tau}^{*})^{\mathrm{T}}]\rangle+\langle u_{x},\tau_{xz}^{*}\rangle\big|_{0}^{1}+\langle u_{y},\tau_{yz}^{*}\rangle\big|_{0}^{1}, \tag{A12}$$

then L_{C}^{*} is given by

$$L_{\mathrm{C}}^{*}=\begin{vmatrix}\Delta&-\boldsymbol{\nabla}&\mathrm{Ra}_{\mathrm{C}}^{\mathrm{S}}\mathbf{e}_{z}&-a\Gamma\\\boldsymbol{\nabla}&0&0&0\\\mathbf{e}_{z}\cdot&0&\Delta&0\\0&0&0&-1\end{vmatrix}. \tag{A13}$$

The corresponding boundary conditions are given by

$$\theta^{*}=u_{z}^{*}=\tau_{xz}^{*}=\tau_{yz}^{*}=0,\quad\text{at } z=0,\ 1. \tag{A14}$$

APPENDIX B: EXPRESSIONS OF τ_0, b, c, d, AND e

The coefficients, τ_0, b, c, d, and e in amplitude equations (33)–(38) are given explicitly as follows:

$$\tau_{0}=\frac{C_{0}(2,1)}{C_{1}(2,1,1)}, \tag{B1}$$

$$b = \left\{\left[C_2\binom{1,1,4}{2,1,42} + C_2\binom{1,4,1}{2,42,1}\right] - \frac{(r-1)C_1(1,2,1)}{s_1^2 C_0(1,2)}\left[C_2\binom{1,2,4}{2,1,42} + C_2\binom{1,4,2}{2,42,1}\right] - \frac{(r-1)C_1(1,3,1)}{s_1^3 C_0(1,3)}\right.$$
$$\left.\times\left[C_2\binom{1,3,4}{2,1,42} + C_2\binom{1,4,3}{2,42,1}\right]\right\}\frac{\left[C_2\binom{4,1,1}{42,2,7} + C_2\binom{4,1,1}{42,7,2}\right]}{s_{42}^4 C_0(42,4)} + \left\{\left[C_2\binom{1,1,5}{2,1,42} + C_2\binom{1,5,1}{2,42,1}\right] - \frac{(r-1)C_1(1,2,1)}{s_1^2 C_0(1,2)}\right.$$
$$\left.\times\left[C_2\binom{1,2,5}{2,1,42} + C_2\binom{1,5,2}{2,42,1}\right] - \frac{(r-1)C_1(1,3,1)}{s_1^3 C_0(1,3)}\left[C_2\binom{1,3,5}{2,1,42} + C_2\binom{1,5,3}{2,42,1}\right]\right\}\frac{\left[C_2\binom{5,1,1}{42,2,7} + C_2\binom{5,1,1}{42,7,2}\right]}{s_{42}^5 C_0(42,5)}$$
$$+ \left\{\left[C_2\binom{1,1,6}{2,1,42} + C_2\binom{1,6,1}{2,42,1}\right] - \frac{(r-1)C_1(1,2,1)}{s_1^2 C_0(1,2)}\left[C_2\binom{1,2,6}{2,1,42} + C_2\binom{1,6,2}{2,42,1}\right] - \frac{(r-1)C_1(1,3,1)}{s_1^3 C_0(1,3)}\right.$$
$$\left.\times\left[C_2\binom{1,3,6}{2,1,42} + C_2\binom{1,6,3}{2,42,1}\right]\right\}\frac{\left[C_2\binom{6,1,1}{42,2,7} + C_2\binom{6,1,1}{42,7,2}\right]}{s_{42}^6 C_0(42,6)} + \left\{\left[C_2\binom{1,1,4}{2,7,9} + C_2\binom{1,4,1}{2,9,7}\right] - \frac{(r-1)C_1(7,2,1)}{s_7^2 C_0(7,2)}\right.$$
$$\left.\times\left[C_2\binom{1,2,4}{2,7,9} + C_2\binom{1,4,2}{2,9,7}\right] - \frac{(r-1)C_1(7,3,1)}{s_7^3 C_0(7,3)}\left[C_2\binom{1,3,4}{2,7,9} + C_2\binom{1,4,3}{2,7,9}\right]\right\}\frac{\left[C_2\binom{4,1,1}{9,2,1} + C_2\binom{4,1,1}{9,1,2}\right]}{s_9^4 C_0(9,4)}$$
$$+ \left\{\left[C_2\binom{1,1,5}{2,7,9} + C_2\binom{1,5,1}{2,9,7}\right] - \frac{(r-1)C_1(7,2,1)}{s_7^2 C_0(7,2)}\left[C_2\binom{1,2,5}{2,7,9} + C_2\binom{1,5,2}{2,9,7}\right] - \frac{(r-1)C_1(7,3,1)}{s_7^3 C_0(7,3)}\left[C_2\binom{1,3,5}{2,7,9}\right.\right.$$
$$\left.\left. + C_2\binom{1,5,3}{2,9,7}\right]\right\}\frac{\left[C_2\binom{5,1,1}{9,2,1} + C_2\binom{5,1,1}{9,1,2}\right]}{s_9^5 C_0(9,5)} + \left\{\left[C_2\binom{1,1,6}{2,7,9} + C_2\binom{1,6,1}{2,9,7}\right] - \frac{(r-1)C_1(7,2,1)}{s_7^2 C_0(7,2)}\right.$$
$$\left.\times\left[C_2\binom{1,2,6}{2,7,9} + C_2\binom{1,6,2}{2,9,7}\right] - \frac{(r-1)C_1(7,3,1)}{s_7^3 C_0(7,3)}\left[C_2\binom{1,3,6}{2,7,9} + C_2\binom{1,6,3}{2,9,7}\right]\right\}\frac{\left[C_2\binom{6,1,1}{9,2,1} + C_2\binom{6,1,1}{9,1,2}\right]}{s_9^6 C_0(9,6)}, \tag{B2}$$

$$c = \left\{\left[C_2\binom{1,1,4}{2,8,62} + C_2\binom{1,4,1}{2,62,8}\right] - \frac{(r-1)C_1(8,2,1)}{s_8^2 C_0(8,2)}\left[C_2\binom{1,2,4}{2,8,62} + C_2\binom{1,4,2}{2,62,8}\right] - \frac{(r-1)C_1(8,3,1)}{s_8^3 C_0(8,3)}\left[C_2\binom{1,3,4}{2,8,62}\right.\right.$$
$$\left.\left. + C_2\binom{1,4,3}{2,62,8}\right]\right\}\frac{C_2\binom{4,1,1}{62,2,2}}{s_{62}^4 C_0(62,4)} + \left\{\left[C_2\binom{1,1,5}{2,8,62} + C_2\binom{1,5,1}{2,62,8}\right] - \frac{(r-1)C_1(8,2,1)}{s_8^2 C_0(8,2)}\left[C_2\binom{1,2,5}{2,8,62} + C_2\binom{1,5,2}{2,62,8}\right]\right.$$
$$\left. - \frac{(r-1)C_1(8,3,1)}{s_8^3 C_0(8,3)}\left[C_2\binom{1,3,5}{2,8,62} + C_2\binom{1,5,3}{2,62,8}\right]\right\}\frac{C_2\binom{5,1,1}{62,2,2}}{s_{62}^5 C_0(62,5)} + \left\{\left[C_2\binom{1,1,6}{2,8,62} + C_2\binom{1,6,1}{2,62,8}\right]\right.$$
$$\left. - \frac{(r-1)C_1(8,2,1)}{s_8^2 C_0(8,2)}\left[C_2\binom{1,2,6}{2,8,62} + C_2\binom{1,6,2}{2,62,8}\right] - \frac{(r-1)C_1(8,3,1)}{s_8^3 C_0(8,3)}\left[C_2\binom{1,3,6}{2,8,62} + C_2\binom{1,6,3}{2,62,8}\right]\right\}\frac{C_2\binom{6,1,1}{62,2,2}}{s_{62}^6 C_0(62,6)}$$
$$+ \left\{\left[C_2\binom{1,2,1}{2,73,2} + C_2\binom{1,1,2}{2,2,73}\right] - \frac{(r-1)C_1(2,2,1)}{s_2^2 C_0(2,2)}\left[C_2\binom{1,2,2}{2,73,2} + C_2\binom{1,2,2}{2,2,73}\right] - \frac{(r-1)C_1(2,3,1)}{s_2^3 C_0(2,3)}\right.$$
$$\left.\times\left[C_2\binom{1,2,3}{2,73,2} + C_2\binom{1,3,2}{2,2,73}\right]\right\}\frac{\left[C_2\binom{2,1,1}{73,2,8} + C_2\binom{2,1,1}{73,8,2}\right]}{s_{73}^2 C_0(73,2)}, \tag{B3}$$

$$d = \left\{\left[C_2\begin{pmatrix}1,1,4\\2,4,56\end{pmatrix} + C_2\begin{pmatrix}1,4,1\\2,56,4\end{pmatrix}\right] - \frac{(r-1)C_1(4,2,1)}{s_{43}^2 C_0(4,2)}\left[C_2\begin{pmatrix}1,2,4\\2,4,56\end{pmatrix} + C_2\begin{pmatrix}1,4,2\\2,56,4\end{pmatrix}\right] - \frac{(r-1)C_1(4,3,1)}{s_4^3 C_0(4,3)}\right.$$
$$\left.\times\left[C_2\begin{pmatrix}1,3,4\\2,4,56\end{pmatrix} + C_2\begin{pmatrix}1,4,3\\2,56,4\end{pmatrix}\right]\right\}\frac{\left[C_2\begin{pmatrix}4,1,1\\56,2,10\end{pmatrix} + C_2\begin{pmatrix}4,1,1\\56,10,2\end{pmatrix}\right]}{s_{56}^4 C_0(56,4)} + \left\{\left[C_2\begin{pmatrix}1,1,5\\2,4,56\end{pmatrix} + C_2\begin{pmatrix}1,5,1\\2,56,4\end{pmatrix}\right]\right.$$
$$- \frac{(r-1)C_1(4,2,1)}{s_4^2 C_0(34,2)}\left[C_2\begin{pmatrix}1,2,5\\2,4,56\end{pmatrix} + C_2\begin{pmatrix}1,5,2\\2,56,4\end{pmatrix}\right] - \frac{(r-1)C_1(4,3,1)}{s_4^3 C_0(4,3)}\left[C_2\begin{pmatrix}1,3,5\\2,4,56\end{pmatrix}\right.$$
$$\left.\left.+ C_2\begin{pmatrix}1,5,3\\2,56,4\end{pmatrix}\right]\right\}\frac{\left[C_2\begin{pmatrix}5,1,1\\56,2,10\end{pmatrix} + C_2\begin{pmatrix}5,1,1\\56,10,2\end{pmatrix}\right]}{s_{56}^5 C_0(56,5)} + \left\{\left[C_2\begin{pmatrix}1,1,6\\2,4,56\end{pmatrix} + C_2\begin{pmatrix}1,6,1\\2,56,4\end{pmatrix}\right] - \frac{(r-1)C_1(4,2,1)}{s_4^2 C_0(4,2)}\right.$$
$$\left.\times\left[C_2\begin{pmatrix}1,2,6\\2,4,56\end{pmatrix} + C_2\begin{pmatrix}1,6,2\\2,56,4\end{pmatrix}\right] - \frac{(r-1)C_1(4,3,1)}{s_4^3 C_0(4,3)}\right.$$
$$\left.\times\left[C_2\begin{pmatrix}1,3,6\\2,4,56\end{pmatrix} + C_2\begin{pmatrix}1,6,3\\2,56,4\end{pmatrix}\right]\right\}\frac{\left[C_2\begin{pmatrix}6,1,1\\56,2,10\end{pmatrix} + C_2\begin{pmatrix}6,1,1\\56,10,2\end{pmatrix}\right]}{s_{56}^6 C_0(56,6)} + \left\{\left[C_2\begin{pmatrix}1,1,4\\2,10,18\end{pmatrix} + C_2\begin{pmatrix}1,4,1\\2,18,10\end{pmatrix}\right]\right.$$
$$- \frac{(r-1)C_1(10,2,1)}{s_{10}^2 C_0(10,2)}\left[C_2\begin{pmatrix}1,2,4\\2,10,18\end{pmatrix} + C_2\begin{pmatrix}1,4,2\\2,18,10\end{pmatrix}\right] - \frac{(r-1)C_1(10,3,1)}{s_{10}^3 C_0(10,3)}\left[C_2\begin{pmatrix}1,3,4\\2,10,18\end{pmatrix}\right.$$
$$\left.\left.+ C_2\begin{pmatrix}1,4,3\\2,18,10\end{pmatrix}\right]\right\}\frac{\left[C_2\begin{pmatrix}4,1,1\\18,2,4\end{pmatrix} + C_2\begin{pmatrix}4,1,1\\18,4,2\end{pmatrix}\right]}{s_{18}^4 C_0(18,4)} + \left\{\left[C_2\begin{pmatrix}1,1,5\\2,10,18\end{pmatrix} + C_2\begin{pmatrix}1,5,1\\2,18,10\end{pmatrix}\right]\right.$$
$$- \frac{(r-1)C_1(10,2,1)}{s_{10}^2 C_0(10,2)}\left[C_2\begin{pmatrix}1,2,5\\2,10,18\end{pmatrix} + C_2\begin{pmatrix}1,5,2\\2,18,10\end{pmatrix}\right] - \frac{(r-1)C_1(10,3,1)}{s_{10}^3 C_0(10,3)}\left[C_2\begin{pmatrix}1,3,5\\2,10,18\end{pmatrix}\right.$$
$$\left.\left.+ C_2\begin{pmatrix}1,5,3\\2,18,10\end{pmatrix}\right]\right\}\frac{\left[C_2\begin{pmatrix}5,1,1\\18,2,4\end{pmatrix} + C_2\begin{pmatrix}5,1,1\\18,4,2\end{pmatrix}\right]}{s_{18}^5 C_0(18,5)} + \left\{\left[C_2\begin{pmatrix}1,1,6\\2,10,18\end{pmatrix} + C_2\begin{pmatrix}1,6,1\\2,18,10\end{pmatrix}\right]\right.$$
$$- \frac{(r-1)C_1(10,2,1)}{s_{10}^2 C_0(10,2)}\left[C_2\begin{pmatrix}1,2,6\\2,10,18\end{pmatrix} + C_2\begin{pmatrix}1,6,2\\2,18,10\end{pmatrix}\right] - \frac{(r-1)C_1(10,3,1)}{s_{10}^3 C_0(10,3)}\left[C_2\begin{pmatrix}1,3,6\\2,10,18\end{pmatrix}\right.$$
$$\left.\left.+ C_2\begin{pmatrix}1,6,3\\2,18,10\end{pmatrix}\right]\right\}\frac{\left[C_2\begin{pmatrix}6,1,1\\18,2,4\end{pmatrix} + C_2\begin{pmatrix}6,1,1\\18,4,2\end{pmatrix}\right]}{s_{18}^6 C_0(18,6)}, \tag{B4}$$

$$e = \left\{\left[C_2\begin{pmatrix}1,1,4\\2,5,32\end{pmatrix} + C_2\begin{pmatrix}1,4,1\\2,32,5\end{pmatrix}\right] - \frac{(r-1)C_1(53,2,1)}{s_4^2 C_0(5,2)}\left[C_2\begin{pmatrix}1,2,4\\2,5,32\end{pmatrix} + C_2\begin{pmatrix}1,4,2\\2,32,5\end{pmatrix}\right] - \frac{(r-1)C_1(5,3,1)}{s_5^3 C_0(5,3)}\right.$$
$$\left.\times\left[C_2\begin{pmatrix}1,3,4\\2,5,32\end{pmatrix} + C_2\begin{pmatrix}1,4,3\\2,32,5\end{pmatrix}\right]\right\}\frac{\left[C_2\begin{pmatrix}4,1,1\\32,2,11\end{pmatrix} + C_2\begin{pmatrix}4,1,1\\32,11,2\end{pmatrix}\right]}{s_{32}^4 C_0(32,4)} + \left\{\left[C_2\begin{pmatrix}1,1,5\\2,5,32\end{pmatrix}\right.\right.$$
$$\left.\left.+ C_2\begin{pmatrix}1,5,1\\2,32,5\end{pmatrix}\right] - \frac{(r-1)C_1(5,2,1)}{s_5^2 C_0(5,2)}\left[C_2\begin{pmatrix}1,2,5\\2,5,32\end{pmatrix} + C_2\begin{pmatrix}1,5,2\\2,32,5\end{pmatrix}\right] - \frac{(r-1)C_1(5,3,1)}{s_5^3 C_0(5,3)}\left[C_2\begin{pmatrix}1,3,5\\2,5,32\end{pmatrix}\right.$$

$$+ C_2\begin{pmatrix}1,5,3\\2,32,5\end{pmatrix}\Bigg]\Bigg\}\frac{\left[C_2\begin{pmatrix}5,1,1\\32,2,11\end{pmatrix}+C_2\begin{pmatrix}5,1,1\\32,11,2\end{pmatrix}\right]}{s_{32}^5C_0(32,5)}$$

$$+\left\{\left[C_2\begin{pmatrix}1,1,6\\2,5,32\end{pmatrix}+C_2\begin{pmatrix}1,6,1\\2,32,5\end{pmatrix}\right]-\frac{(r-1)C_1(5,2,1)}{s_5^2C_0(5,2)}\left[C_2\begin{pmatrix}1,2,6\\2,5,32\end{pmatrix}+C_2\begin{pmatrix}1,6,2\\2,32,5\end{pmatrix}\right]-\frac{(r-1)C_1(5,3,1)}{s_5^3C_0(5,3)}\right.$$

$$\left.\times\left[C_2\begin{pmatrix}1,3,6\\2,5,32\end{pmatrix}+C_2\begin{pmatrix}1,6,3\\2,32,5\end{pmatrix}\right]\right\}\frac{\left[C_2\begin{pmatrix}6,1,1\\32,2,11\end{pmatrix}+C_2\begin{pmatrix}6,1,1\\32,11,2\end{pmatrix}\right]}{s_{32}^6C_0(32,6)}+\left\{\left[C_2\begin{pmatrix}1,1,4\\2,11,35\end{pmatrix}+C_2\begin{pmatrix}1,4,1\\2,35,11\end{pmatrix}\right]\right.$$

$$\left.-\frac{(r-1)C_1(11,2,1)}{s_{11}^2C_0(11,2)}\left[C_2\begin{pmatrix}1,2,4\\2,11,35\end{pmatrix}+C_2\begin{pmatrix}1,4,2\\2,35,11\end{pmatrix}\right]-\frac{(r-1)C_1(11,3,1)}{s_{11}^3C_0(11,3)}\left[C_2\begin{pmatrix}1,3,4\\2,11,35\end{pmatrix}+C_2\begin{pmatrix}1,4,3\\2,35,11\end{pmatrix}\right]\right\}$$

$$\times\frac{\left[C_2\begin{pmatrix}4,1,1\\35,2,5\end{pmatrix}+C_2\begin{pmatrix}4,1,1\\35,5,2\end{pmatrix}\right]}{s_{35}^4C_0(35,4)}+\left\{\left[C_2\begin{pmatrix}1,1,5\\2,11,35\end{pmatrix}+C_2\begin{pmatrix}1,5,1\\2,35,11\end{pmatrix}\right]-\frac{(r-1)C_1(11,2,1)}{s_{11}^2C_0(11,2)}\right.$$

$$\left.\times\left[C_2\begin{pmatrix}1,2,5\\2,11,35\end{pmatrix}+C_2\begin{pmatrix}1,5,2\\2,35,11\end{pmatrix}\right]-\frac{(r-1)C_1(11,3,1)}{s_{11}^3C_0(11,3)}\left[C_2\begin{pmatrix}1,3,5\\2,11,35\end{pmatrix}+C_2\begin{pmatrix}1,5,3\\2,35,11\end{pmatrix}\right]\right\}$$

$$\times\frac{\left[C_2\begin{pmatrix}5,1,1\\35,2,5\end{pmatrix}+C_2\begin{pmatrix}5,1,1\\35,5,2\end{pmatrix}\right]}{s_{35}^5C_0(35,5)}+\left\{\left[C_2\begin{pmatrix}1,1,6\\2,11,35\end{pmatrix}+C_2\begin{pmatrix}1,6,1\\2,35,11\end{pmatrix}\right]-\frac{(r-1)C_1(11,2,1)}{s_{11}^2C_0(11,2)}\right.$$

$$\left.\times\left[C_2\begin{pmatrix}1,2,6\\2,11,35\end{pmatrix}+C_2\begin{pmatrix}1,6,2\\2,35,11\end{pmatrix}\right]-\frac{(r-1)C_1(11,3,1)}{s_{11}^3C_0(11,3)}\left[C_2\begin{pmatrix}1,3,6\\2,11,35\end{pmatrix}+C_2\begin{pmatrix}1,6,3\\2,35,11\end{pmatrix}\right]\right\}$$

$$\times\frac{\left[C_2\begin{pmatrix}6,1,1\\35,2,5\end{pmatrix}+C_2\begin{pmatrix}6,1,1\\35,5,2\end{pmatrix}\right]}{s_{35}^6C_0(35,6)}. \tag{B5}$$

[1] H. Bénard, Rev. Sci. **11**, 1261 (1900); **11**, 1309 (1900).
[2] Lord Rayleigh, Philos. Mag. **32**, 529 (1916).
[3] E. L. Koschmieder, *Bénard Cells and Taylor Vortices* (Cambridge University Press, New York, 1993).
[4] T. Green, Phys. Fluids **11**, 1410 (1968).
[5] C. M. Vest and V. S. Arpaci, J. Fluid Mech. **36**, 613 (1969).
[6] M. Sokolov and R. I. Tanner, Phys. Fluids **15**, 534 (1972).
[7] I. A. Eltayeb, Proc. R. Soc. London, Ser. A **356**, 161 (1977).
[8] S. Rosenblat, J. Non-Newtonian Fluid Mech. **21**, 201 (1986).
[9] J. Martínez-Mardones and C. Pérez-García, II Nuovo Cimento **14**, 961 (1992).
[10] H. Harder, J. Non-Newtonian Fluid Mech. **36**, 67 (1991).
[11] R. E. Khayat, J. Non-Newtonian Fluid Mech. **53**, 227 (1994).
[12] R. E. Khayat, J. Non-Newtonian Fluid Mech. **58**, 331 (1995).
[13] R. E. Khayat, Phys. Rev. E **51**, 380 (1995).
[14] R. E. Khayat, J. Non-Newtonian Fluid Mech. **63**, 153 (1996).
[15] H. M. Park and H. S. Lee, J. Non-Newtonian Fluid Mech. **66**, 1 (1996).
[16] J. Martínez-Mardones, R. Tiemann, D. Walgraef, and W. Zeller, Phys. Rev. E **54**, 1478 (1996).
[17] P. Parmentier, G. Lebon, and V. Regnier, J. Non-Newtonian Fluid Mech. **89**, 63 (2000).
[18] S. F. Liang and A. Acrivos, Rheol. Acta **9**, 447 (1970).
[19] P. Kolodner, J. Non-Newtonian Fluid Mech. **75**, 167 (1998).
[20] S. Chandrasekhar, *Hydrodynamic and Hydromagnetic Stability* (Dover Publications, New York, 1961).
[21] R. B. Bird, R. C. Armstrong, and O. Hassage, *Dynamics of Polymeric Liquids*, 2nd edition (John Wiley & Sons, New York, 1987), Vol. 1.
[22] U. A. Al-Mubaiyedh, R. Sureshkumar, and B. Khomami, Phys. Fluids **11** 3217 (1999).
[23] P. G. Drazin and W. H. Reid, *Hydrodynamic Stability* (Cambridge University Press, New York, 1981).
[24] B. Friedman, *Principles and Techniques of Applied Mathematics* (John Wiley & Sons, New York, 1956).
[25] W. Eckhaus, *Studies in Non-linear Stability Theory* (Springer, New York, 1965).
[26] A. C. Newell, T. Passot, and J. Lega, Annu. Rev. Fluid Mech. **25**, 399 (1993).
[27] M. C. Cross and P. C. Hohenherg, Rev. Mod. Phys. **65**, 851 (1993).
[28] A. Schlüter, D. Lortz, and F. Busse, J. Fluid Mech. **23**, 130 (1965).